Computers and Concrete, *Vol. 13, No. 1 (2014) 49-70*
DOI: http://dx.doi.org/10.12989/cac.2014.13.1.049

Application of direct tension force transfer model with modified fixed-angle softened-truss model to finite element analysis of steel fiber-reinforced concrete members subjected to Shear

Deuck Hang Lee[a], Jin-Ha Hwang[b], Hyunjin Ju[c] and Kang Su Kim[*]

Department of Architectural Engineering, University of Seoul, 90 Jeonnong-dong, Dongdaemun-gu, Seoul 130-743, Republic of Korea

(*Received February 12, 2012, Revised April 1, 2013, Accepted July 30, 2013*)

Abstract. Steel fiber-reinforced concrete (SFRC) is known as one of the efficient modern composites that can greatly enhance the material performance of cracked concrete in tension. Such improved tensile resistance mechanism at crack interfaces in SFRC members can be heavily influenced by methodologies of treatments of crack direction. While most existing studies have focused on developing the numerical analysis model with the rotating-angle theory, there are only few studies on finite element analysis models with the fixed-angle model approach. According to many existing experimental studies, the direction of principal stress rotated after the formation of initial fixed-cracks, but it was also observed that new cracks with completely different angles relative to the initial crack direction very rarely occurred. Therefore, this study introduced the direct tension force transfer model (DTFTM), in which tensile resistance of the fibers at the crack interface can be easily estimated, to the nonlinear finite element analysis algorithm with the fixed-angle theory, and the proposed model was also verified by comparing the analysis results to the SFRC shear panel test results. The secant modulus method adopted in this study for iterative calculations in nonlinear finite element analysis showed highly stable and fast convergence capability when it was applied to the fixed-angle theory. The deviation angle between the principal stress direction and the fixed-crack direction significantly increased as the tensile stresses in the steel fibers at crack interfaces increased, which implies that the deviation angle is very important in the estimation of the shear behavior of SFRC members.

Keywords: fixed angle; nonlinear analysis; finite element; SFRC; shear; DTFTM; steel fiber; deviation angle; pullout failure

1. Introduction

The concrete has become the most popular material in modern civil engineering and construction markets with its cost-effectiveness and excellence in forming the various shape of

∗Corresponding author, Associate Professor, E-mail: kangkim@uos.ac.kr
[a]Ph.D. Candidate, E-mail: dklee@uos.ac.kr
[b]Ph.D. Candidate, E-mail: asorange@nate.com
[c]Ph.D. Candidate, E-mail: fis00z@uos.ac.kr

http://www.techno-press.org/?journal=cac&subpage=8 ISSN: 1598-8198 (Print), 1598-818X (Online)

structure. Compared to other homogeneous materials like steel, however, concrete composed of cement, aggregates, and other admixtures has very complicated structural behavior, and its brittle material characteristic also often causes the issues on degradation of serviceability due to various types of cracks (ACI-ASCE Committee 445 1999, ACI Committee 544 1988, Neville 1996). Therefore, to resolve the such deficiency of concrete material, various types of cement composites have been developed, and particularly, there are growing interests in research and design applications of steel fiber-reinforced concrete (SFRC), which mixes short and small-diameter fibers with cement to improve the poor tensile performance of conventional concrete (Janis 2008, Kim *et al*. 2012, Romualdi and Mandel 1964, Lee *et al*. 2012). Despite the remarkable advancements in analysis technologies for concrete structures since the twentieth century, however, there still has been lack of understanding in the shear behavior of SFRC members due to the complex mechanism of the tensile resistance of steel fibers at crack, which is randomly distributed in concrete. Most of the tensile behavior models of fibers at the crack interfaces utilized the macroscopic concept using a fully-composite-based tensile behavior model based on uniaxial tensile tests or shear panel tests of SFRC (Abrishami and Mitchell 1997; Lim *et al*. 1987, Tan and Mansur 1990, Tan *et al*. 1992). These macroscopic models require numerous test data for calibration, and have some difficulties in describing the realistic tensile resistance of fibers at the crack interfaces, such as bond behavior developed between fibers and surrounding concrete or pull-out failure of fibers. In the previous studies of authors, the direct tension force transfer model (DTFTM) was proposed (Kim *et al*. 2013, Lee *et al*. 2012, Hwang *et al*. 2013, Ju *et al*. 2013a and 2013b) in which steel fibers were modeled as the direct tension resistance elements at crack surfaces in a microscopic level. Because the tensile contribution of steel fibers is determined by the steel fibers at the crack interfaces, the shear strength and behavior of SFRC is largely dependent on the angle of inclination of crack (i.e. crack direction) and its width as well as the directionality and random distribution characteristics of fibers. Once cracks are initiated in a concrete member, they typically do not rotate significantly from the initial crack direction, and instead, often tend to propagate further with increasing their widths. Thus, the application of the rotating-angle theory to the direct tension force transfer model may result in somewhat unrealistic analytical results. In this study, therefore, the shear behavior of SFRC members was estimated utilizing a nonlinear finite element analysis algorithm based on the fixed-angle theory (Hsu and Mo 2010, Pang and Hsu 1996, Wang and Hsu 2001), and its numerical and mechanical characteristics were also discussed in detail.

2. Research significance

Among the shear resistance mechanisms of steel fiber reinforced concrete (SFRC) members, the contribution of steel fibers in tension at crack interfaces is largely dependent on the methodology of treatments of crack direction and distribution. To reflect the tensile behavior of steel fibers at crack interfaces in the analysis more realistically than the models based on the rotating-angle theory, this study developed a nonlinear finite element analysis algorithm based on the fixed-angle theory and the direct tension force transfer model. The proposed numerical analysis model reasonably estimated the overall shear behavior and deformation capacity of SFRC members, and the relationships between the tensile contribution of steel fibers at the crack surfaces and the deviation angle were also evaluated from the analysis results.

3. Background

Since there is a lack of clear understanding in the shear behavior of concrete structural members, many studies on this subject are still consistently being investigated (ACI-ASCE•Committee 445 1999, Hsu and Mo 2010). Factors that make the shear analysis of the concrete structural members difficult are the occurrence of cracks due to the brittle nature of concrete materials, crack growth, and its directionality (Chen 1982, Kim *et al*. 2011). As shown in Fig. 1, depending on the treatment methods of cracks, the shear behavior analysis model of concrete structural members can be generally divided into the discrete cracking model and the smeared cracking model (Chen 1982, Hu and Schnobrich 1990, Ngo and Scordelis 1967). The modified compression field theory (MCFT) and the softened truss model (STM), which are the most widely used shear theories among developed so far, correspond to the smeared cracking model, and as shown in Fig. 2, they can be divided further into the fixed-angle model (Hsu and Mo 2010, Pang and Hsu 1996, Wang and Hsu 2001) and the rotating-angle model (Vecchio 1989, Vecchio 1990, Vecchio and Collins 1986) based on the method in consideration of the direction of the cracks. The differences between these theories can be clearly understood by examining the stress and strain distributions of the concrete wedge elements and the corresponding Mohr's stress and strain circles shown in Fig. 3. Since the rotating-angle theory assumes that the direction of the principal strain is identical to that of the principal stress, the crack directions in rotating-angle model change continuously, following the rotation of the principal tensile strain direction as the external shear force increases. That is, it assumes that the damages by tensile cracking in concrete, which actually occurred in the previous principal stress direction, are rotated and accumulated to the current principal stress direction in accordance with the change in the direction of the principal stress. The direction of the principal stress in concrete member after shear cracking gradually changes due to various reasons, such as the redistribution of internal stresses, the asymmetrical

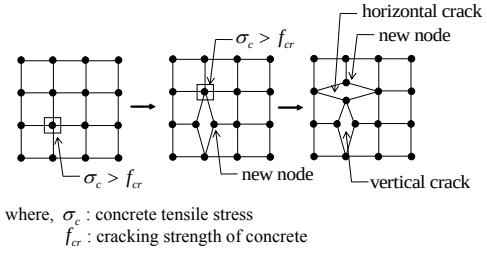

(a) Discrete-cracking model

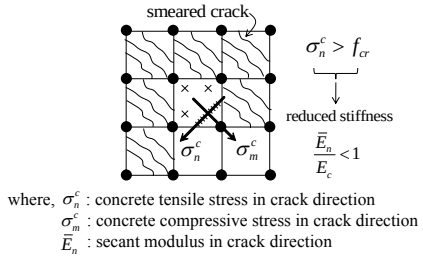

(b) Smeared-cracking model

Fig. 1 Cracking models

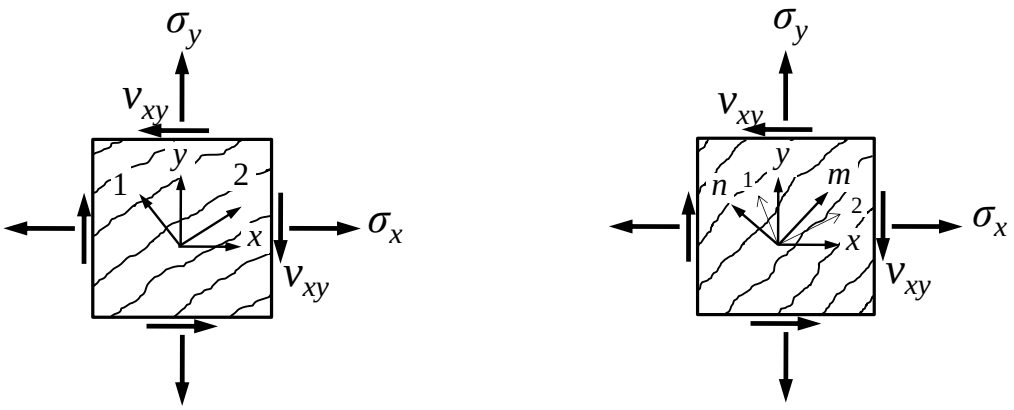

(a) Rotating-angle model (b) Fixed-angle model

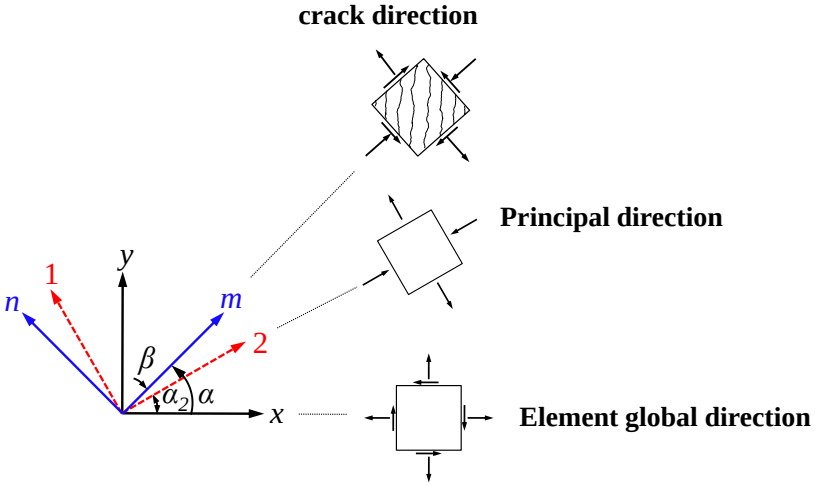

(c) Definition of coordinate systems and deviation angle

Fig. 2 Differences between the rotating-angle model and the fixed-angle model

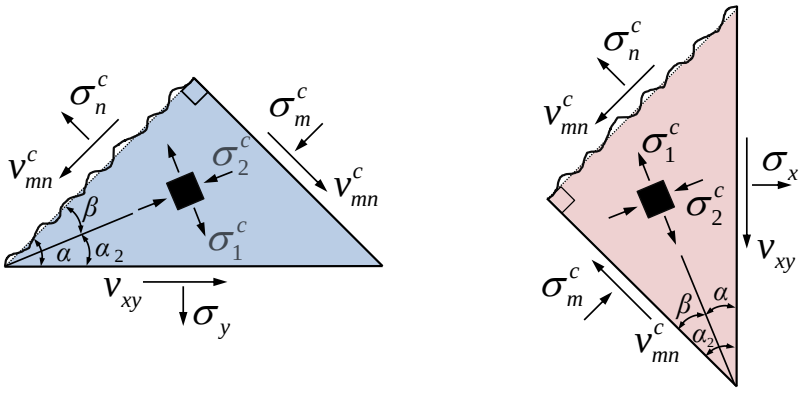

(a) Stress distribution in the fixed-angle model

Fig. 3 Differences between the rotating-angle model and the fixed-angle model

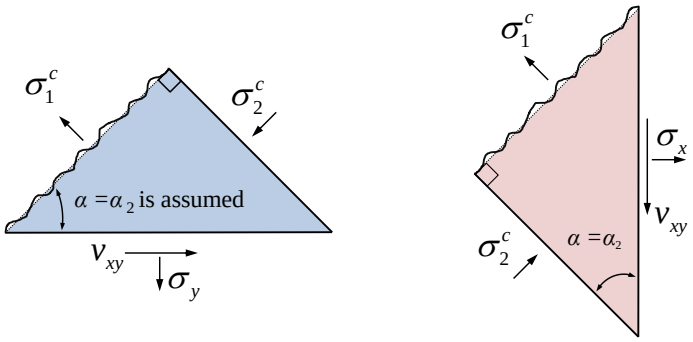

(b) Stress distribution in the rotating-angle model

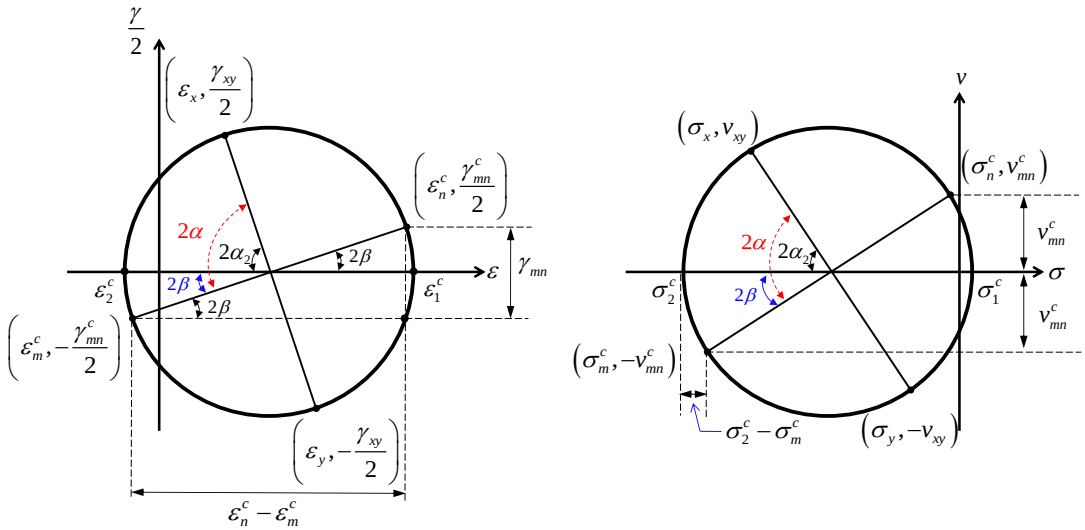

(c) Mohr's strain circle (d) Mohr's stress circle

Fig. 3 Continued

distribution of reinforcements in orthogonal directions, loading configurations, etc. When the direction of the principal stress gradually changes, it is possible to form a few small tensile cracks in perpendicular to the current principal tensile stress direction, which are distinctive to the previously formed tensile cracks. However, the existing cracks previously formed in the concrete member typically propagate in a more intensive manner and their crack widths become larger (Kim *et al*. 2012). Therefore, based on such a theoretical and experimental observations, fixed-angle theories have been developed (Hsu and Mo 2010, Pang and Hsu 1996, Wang and Hsu 2001), where the direction of the principal strain (or the initial crack direction) does not coincide with the direction of the principal stress. Therefore, the aggregate interlocking action at the crack surfaces, which has been known as a primary shear resistance mechanism in structural concrete member, can be reasonably considered in shear behavior analysis (Hsu 1998). In the authors' previous studies (Hwang *et al*. 2012, Kim *et al*. 2012), the direct tension force transfer model (DTFTM) that considered different bond strengths according to fiber types was proposed, in which the randomly distributed steel fibers were modeled as direct tensile resistance elements and converted into the effective cross-sectional area of fibers that exists in the perpendicular to the crack interfaces.

Furthermore, the nonlinear finite element analysis algorithm on the basis of the rotating angle theory (Lee *et al*. 2012) was proposed and its theoretical rationality and accuracy was also validated. As previously mentioned, however, the analysis on the behavior of steel fibers at the crack interface is largely dependent on the methodology of considering the crack direction and distribution (Lee *et al*. 2011, Voo and Foster 2003). This study, therefore, aimed to develop the finite element analysis method in which DTFTM is applied to the fixed-angle theory in order to consider more details in the tensile resistance of the steel fibers at the crack surface where the pull-out failure of fibers occurs, and shear behavior of SFRC members was also evaluated quantitatively by the proposed analysis model.

4. Direct tension force transfer model with fixed-angle approach

As shown in Fig. 4(a), it can be assumed that a certain number of steel fibers resists tensile stress in perpendicular to the crack surface, and that steel fibers show completely composite action with concrete surrounding it until bond resistance between fibers and concrete is lost. For simplicity, therefore, the stress of the steel fiber, before it reaches to the ultimate bond strength ($\tau_{\max}$), can be expressed as

$$\sigma_n^{sf} = E_{sf}\varepsilon_n^c \tag{1}$$

where σ_n^{sf} is the stress of the steel fiber, E_{sf} is the modulus of elasticity of the steel fiber, for which this study used 200 GPa, ε_n^c is the tensile strain of concrete in the perpendicular direction to the crack surface. Since not all of the steel fibers at the crack surface resist in the principal tensile stress direction, the average tensile stress in steel fibers, which are effective at the crack surface, should be estimated. If the number of steel fibers at the crack interface (*n*-direction in Fig. 4) is designated as n_f, the average tensile stress of steel fibers ($\sigma_{n,ave}^{sf}$) at the crack surface can be expressed, as follows

$$\sigma_{n,ave}^{sf} = \frac{T_{sf}}{A_{cs}} = \frac{\sigma_n^{sf} n_f A_{sf}}{A_{cs}} \tag{2}$$

where T_{sf} is the tension force that the steel fibers resist at the crack interface, A_{cs} is the area of the inclined crack surface, and A_{sf} is the cross-sectional area of a steel fiber. Also, the number of steel fibers across the crack (n_f) can be expressed as

$$n_f = n_w A_{cs} \tag{3}$$

where n_w is the number of steel fibers per unit area of the crack interface. In this study, $\lambda V_f / A_{sf}$ is used for n_w, as proposed by Romualdi and Mandel (1964) and Soroushian and Lee (1990), where V_f is the volume fraction of steel fibers, and λ is the fiber orientation factor in

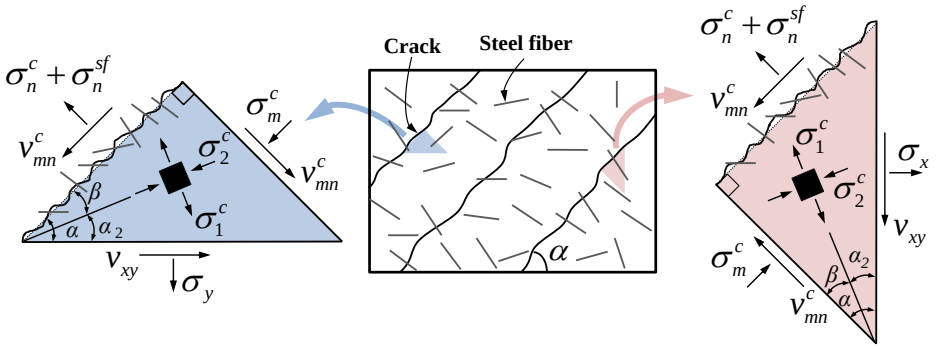

(a) Steel fibers in a SFRC member

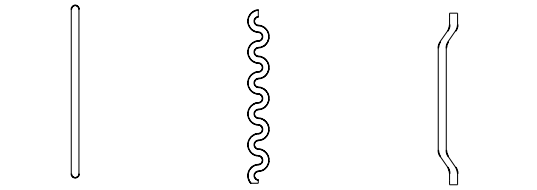

(b) Types of steel fibers and their corresponding shape factors

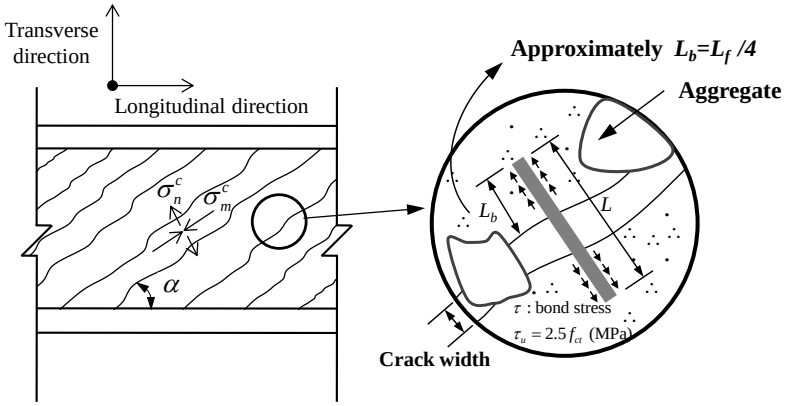

(c) Inclined cracks and steel fibers at crack interfaces

Fig. 4 Concept of the direct tension force transfer model (DTFTM)

an arbitrary space, for which this study used 0.41, as proposed by Romualdi and Mandel (1964). When the number of effective fibers that resists in tension at the crack interface calculated by Eq. (3) is substituted to Eq. (2), the average stress of the steel fibers at the crack surface ($\sigma_{n,ave}^{sf}$) can be modified, as follows:

$$\sigma_{n,ave}^{sf} = 0.41\sigma_n^{sf} V_f \tag{4}$$

Meanwhile, as bond test results of SFRC reported by Lim *et al*. (1987), once the bond stress

between fibers and surrounding concrete reaches to the ultimate bond stress, the tensile stress in the steel fibers no longer increases due to pull-out failure of fibers. Thus, the maximum stress of the steel fibers ($\sigma_{n,\max}^{sf}$) limited by the ultimate bond stress is

$$\sigma_{n,\max}^{sf} = \frac{\tau_{\max} A_{fp} n_f}{A_{cs}} \tag{5}$$

where $\tau_{\max}$ is the maximum bond stress of steel fibers, and A_{fp} is the average surface area of steel fibers on which the bond stress is developed. In this study, $2.5 f_{ct}$ was used for the bond strength of steel fibers (τ_u), as proposed by Voo and Foster (2003), and $0.33\sqrt{f_c'}$ was used for the concrete tensile strength (f_{ct}). Since the bond strengths of the steel fibers are different according to their mechanical shape, the maximum bond strength ($\tau_{\max}$) can be expressed by introducing the shape coefficient of fiber (d_f), as follows

$$\tau_{\max} = \tau_u d_f \tag{6}$$

where, as shown in Fig. 4(b), the shape coefficient of fibers is 1.0 for hooked type, 0.75 for crimped type, and 0.5 for straight type, as proposed by Narayanan and Darwish (1987). Therefore, the maximum stress of the steel fibers ($\sigma_{n,\max}^{sf}$) in Eq. (5) can be expressed, as follows

$$\sigma_{n,\max}^{sf} = \frac{\tau_u d_f A_{fp} n_f}{A_{cs}} \tag{7}$$

However, due to the random distribution of the steel fibers, it is difficult to estimate the length of the steel fibers embedded in concrete after cracking. As shown in Fig. 4(c), therefore, this study assumed ¼ of the fiber length to be the average embedded length, and the maximum stress of the steel fibers ($\sigma_{n,\max}^{sf}$) is determined as follows

$$\sigma_{n,\max}^{sf} = 0.41 V_f \tau_{\max} \frac{L_f}{D} \tag{8}$$

where D and L_f are the diameter and the length of the steel fibers, respectively.

5. Constitutive models and material stiffness matrix

The stress (σ)-strain (ε) relationship of the linear elastic isotropic material in plane stress state is defined (Logan 2007, Smith and Griffiths 2004), as follows:

$$\{\sigma\} = [D_e]\{\varepsilon\} \tag{9a}$$

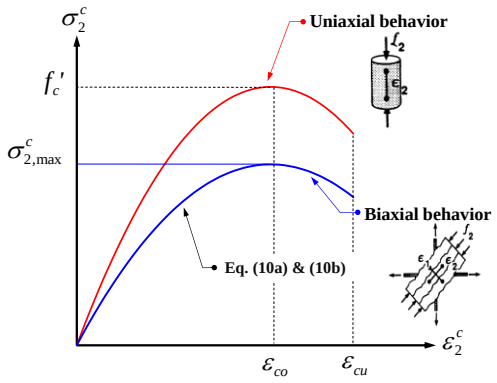

(a) Concrete compressive stress-strain relationship

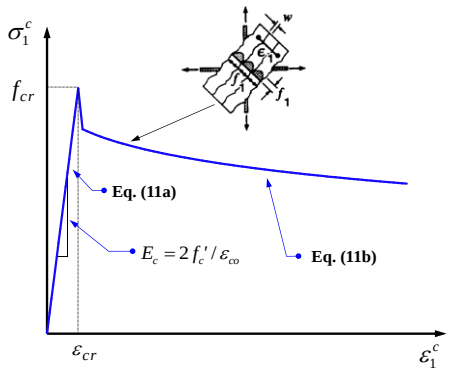

(b) Concrete tensile stress-strain relationship

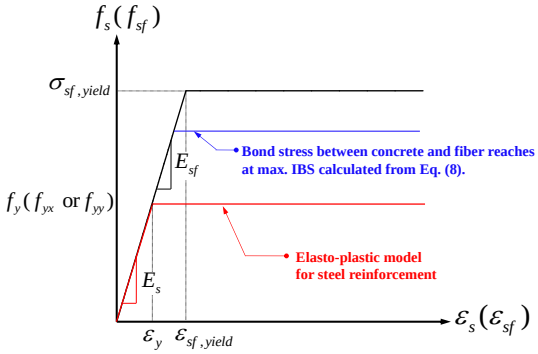

(c) Inclined cracks and steel fibers at crack interfaces

Fig. 5 Stress-strain relationship of materials

$$\begin{Bmatrix}\sigma_x\\ \sigma_y\\ v_{xy}\end{Bmatrix}=\frac{E_c}{(1-\nu^2)}\begin{bmatrix}1 & \nu & 0\\ \nu & 1 & 0\\ 0 & 0 & (1-\nu)/2\end{bmatrix}\begin{Bmatrix}\varepsilon_x\\ \varepsilon_y\\ \gamma_{xy}\end{Bmatrix} \tag{9b}$$

where $[D_e]$ is the stiffness matrix of the linear elastic material. As shown in Fig. 5(a), Popovics model (Popovics 1973) was used as the constitutive equation of the concrete in the principal compressive stress direction of SFRC in this research. In this model, the average principal compressive stress (σ_2), considering the softening effect (Vecchio and Collins, 1986), is expressed as follows

$$\sigma_2^c=\sigma_{2,\max}^c\left[\frac{n\left(\varepsilon_2^c/\varepsilon_{co}\right)}{n-1+\left(\varepsilon_2^c/\varepsilon_{co}\right)^{nk}}\right] \tag{10a}$$

$$\sigma_{2,\max}^{c} = \frac{-f_c'}{0.8 - \dfrac{0.34\varepsilon_1^c}{\varepsilon_{co}}} \geq -f_c' \tag{10b}$$

where ε_2^c is the average principal compressive strain, ε_{co} is the strain corresponding to concrete compressive strength (f_c'), n is $0.8 + f_c'/17$, and k is $0.67 + f_c'/62 \geq 1$. As shown in Fig. 5(b), the tension stiffening model proposed by Vecchio and Collins (1986) were used for the tensile stress-strain relationship of the concrete, as follows:

$$\sigma_1^c = E_c \varepsilon_1^c, \qquad 0 \leq \varepsilon_1^c \leq \varepsilon_{cr} \tag{11a}$$

$$\sigma_1^c = \frac{f_{cr}}{1 + \sqrt{200\varepsilon_1^c}}, \qquad \varepsilon_{cr} \leq \varepsilon_1^c \tag{11b}$$

where σ_1^c and ε_1^c are the average principal tensile stress and strain in concrete, respectively, E_c is the modulus of elasticity of the concrete ($= 2f_c'/\varepsilon_{co}$), f_{cr} and ε_{cr} are the cracking stress ($= 0.33\sqrt{f_c'}$) and strain (f_{cr}/E_c) of the concrete, respectively. As shown in Fig. 5(c), the elasto-perfectly plasticity behavior was assumed for stress-strain relationship of reinforcement. In order to apply the fixed-angle model, the initial crack angle shown in Fig. 2 and Fig. 3 should be determined. According to the studies by Hsu and Wang (2001) and Lee *et al*. (2011), the angle of inclination of the principal stress (α_2) can be estimated, as follows

$$\tan(2\alpha_2) = \frac{2v_{xy}}{\sigma_x - \sigma_y} \tag{12}$$

Once a shear crack is occurred in a concrete member, this angle of inclination of the initial crack is permanently fixed. From Fig. 3, the deviation angle (β) between the initial crack direction and the principal stress direction can be estimated, as follows

$$\beta = \alpha - \alpha_2 \tag{13}$$

As shown in Fig. 2(c) and Fig. 6, the stresses and strains in the crack direction (*n-m* direction) can be calculated by transforming those in the principal stress direction (*1-2* direction) by the deviation angle (β), as in

$$\begin{Bmatrix} \sigma_m^c \\ \sigma_n^c \end{Bmatrix} = \begin{bmatrix} \cos^2\beta & \sin^2\beta \\ \sin^2\beta & \cos^2\beta \end{bmatrix} \begin{Bmatrix} \sigma_2^c \\ \sigma_1^c \end{Bmatrix} \tag{14}$$

$$\begin{Bmatrix} \varepsilon_m^c \\ \varepsilon_n^c \end{Bmatrix} = \begin{bmatrix} \cos^2\beta & \sin^2\beta \\ \sin^2\beta & \cos^2\beta \end{bmatrix} \begin{Bmatrix} \varepsilon_2^c \\ \varepsilon_1^c \end{Bmatrix} \tag{15}$$

The average tensile stress of steel fibers in the crack direction is determined by DTFTM as

explained in previous section, as follows

$$\sigma_{n,ave}^{sf} = 0.41\sigma_n^{sf} V_f \le \sigma_{n,\max}^{sf} \tag{16}$$

The secant stiffness matrix of the steel fiber-reinforced concrete in the crack direction can be derived by combining the secant stiffness of steel fibers ($\bar{E}_n^{sf}$) and that of concrete ($\bar{E}_{cn}$), as follows:

$$\left[D_c\right]'_{n-m} = \begin{bmatrix} \bar{E}_{cn}' & 0 & 0 \\ 0 & \bar{E}_{cm}' & 0 \\ 0 & 0 & \bar{G}_{mn}' \end{bmatrix} = \begin{bmatrix} \bar{E}_{cn} + \bar{E}_n^{sf} & 0 & 0 \\ 0 & \bar{E}_{cm} & 0 \\ 0 & 0 & \dfrac{\bar{E}_{cm}\left(\bar{E}_{cn} + \bar{E}_n^{sf}\right)}{\bar{E}_{cn} + \bar{E}_n^{sf} + \bar{E}_{cm}} \end{bmatrix} \tag{17}$$

where $\bar{E}_n^{sf}$ is the secant stiffness of steel fibers, calculated by $\sigma_{n,ave}^{sf} / \varepsilon_n^c$. Also, $\bar{E}_{cn}$ and $\bar{E}_{cm}$ are the secant stiffness of concrete in the initial crack direction, respectively, which can be calculated by $\sigma_n^c / \varepsilon_n^c$ and $\sigma_m^c / \varepsilon_m^c$, respectively.

5.1 Composite material stiffness matrix

The stiffness matrix of reinforcing bars placed in arbitrary direction ($\left[D_s\right]_i'$) can be expressed as

$$\left[D_s\right]_i' = \begin{bmatrix} \rho_i \bar{E}_{si} & 0 & 0 \\ 0 & 0 & 0 \\ 0 & 0 & 0 \end{bmatrix} \tag{18}$$

where ρ_i is, as shown in Fig. 6(c), the reinforcement ratio in the *i* th direction, and $\bar{E}_{si}$ is the secant stiffness of the reinforcing bar in the *i* th direction, which is estimated by $\bar{E}_{si} = f_{si} / \varepsilon_{si}$. Therefore, by considering the local element coordinate system and the direction of reinforcing bars, the material stiffness matrix in the global coordinate system, $\left[D\right]$, is expressed, as follows

$$\left[D\right] = \left[D_c\right] + \sum_{i=1}^{n} \left[D_s\right]_i \tag{19}$$

where $\left[D_s\right]_i$ is the stiffness matrix of the reinforcing bar in the global coordinate system, which is

$$\left[D_s\right]_i = \left[T\right]_i^t \left[D_s\right]_i' \left[T\right]_i \tag{20}$$

The stiffness matrix of the concrete in the global coordinate system, $\left[D_c\right]$, can be also estimated, as follows

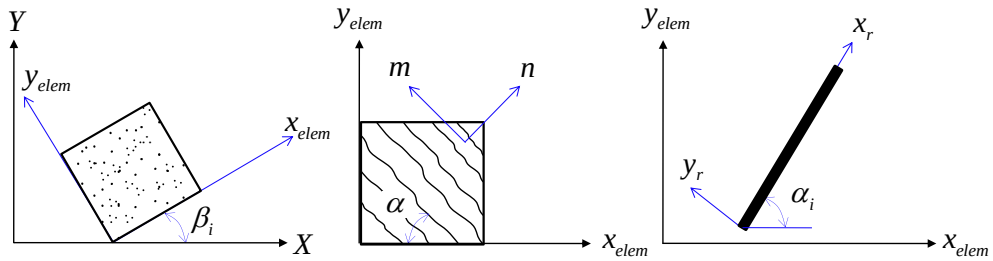

a) Element coordinate system (b) concrete element (c) Reinforcing bars

Fig. 6 Coordinate system in the finite element analysis

$$[D_c] = [T]^t [D_c]'_{n-m} [T] \tag{21}$$

In Eq. (20) and Eq. (21), the transformation matrix ($[T]$) is defined as:

$$[T] = \begin{bmatrix} \cos^2\zeta & \sin^2\zeta & \cos\zeta\sin\zeta \\ \sin^2\zeta & \cos^2\zeta & -\cos\zeta\sin\zeta \\ -2\cos\zeta\sin\zeta & 2\cos\zeta\sin\zeta & \cos^2\zeta - \sin^2\zeta \end{bmatrix} \tag{22}$$

The angle ζ is defined for the reinforcement and concrete element, respectively, as follows:

$$\zeta = \alpha_i + \beta_i \tag{23}$$

$$\zeta = 180 + \beta_i - \alpha \tag{24}$$

where, as shown in Fig. 6, α_i is the angle between reinforcing bar and the global coordinate system, and β_i is the angle between the global coordinate system and local coordination of each concrete element.

5.2 Element stiffness matrix

As shown in Fig. 7, this study used four-node isotropic element, and the coordinate of each node is designated as $x_i, y_i \, (i = 1 \sim 4)$. The stiffness matrix of the four-node isotropic element ($[k]$) can be expressed (Bathe 1996, Yang 1986), as follows

$$[k] = \int [B]^t [D][B] dV \tag{25}$$

where $[B]$ is the shape matrix. To derive the element stiffness matrix, numerical integrations on Eq. (25) should be performed using a four-point Gaussian quadrate.

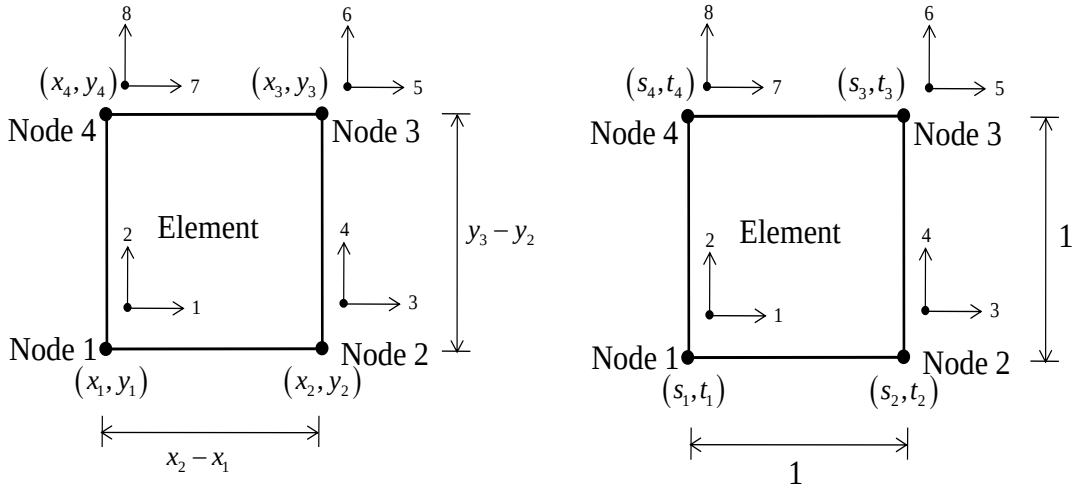

(a) Element in original coordination (b) Element in natural coordination

Fig. 7 4-node isotropic element

6. Implementation of iteration method for nonlinear analysis

Fig. 8 shows the detailed process of the nonlinear analysis of the steel fiber-reinforced concrete member. As aforementioned, the secant stiffness iteration method (Lee *et al*. 2012, Vecchio 1989 and 1990), which has excellent convergence capability and stability in the iterative computational procedures, was applied in this study. In a loading stage, based on elastic material stiffness in Eq. (9), element stiffness is determined, and by combining the stiffness matrix ($[k]_i$) of each element, the total stiffness matrix ($[K]$) can be constructed, as follows

$$[K] = \sum_{i=1}^{k} [k]_i \tag{26}$$

Then, the nodal displacement matrix ($\{\Delta\}$) can be estimated by

$$\{\Delta\} = [K]^{-1} \{F\} \tag{27}$$

where $\{F\}$ is the force matrix.

The strains can be determined by the nodal displacements and the nonlinear stress-strain relationships, from which the stresses and the secant moduli of each element are estimated, and by comparing it to the secant moduli in the previous stage of the iterative calculation process, its convergence is checked. If a certain level of convergence is not achieved, the secant moduli are updated, and the repetitive calculation process is re-performed. Once the imposed convergence condition is satisfied, the strain of each node can be determined based on the calculated nodal displacements, and the average strains and average stresses of the elements can be estimated from the average value of the calculated nodal strains.

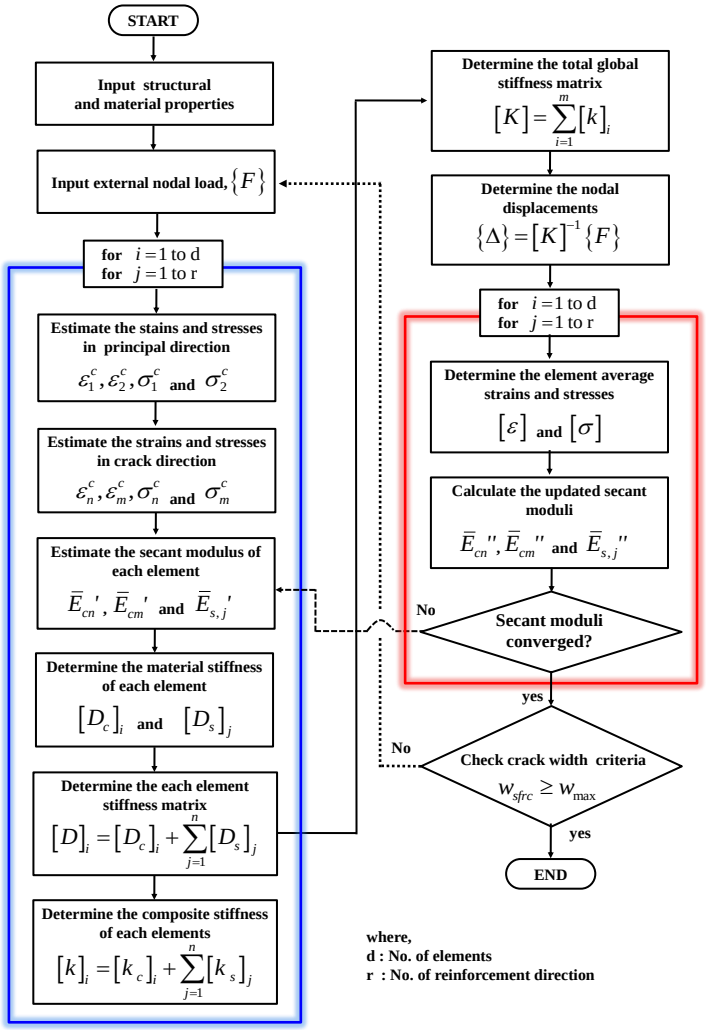

Fig. 8 Analysis procedure of the NLFEM with DTFTM

6. Pull-out failure criteria of SFRC

Steel fibers typically have high tensile strength over 1000 MPa. However, once the bond stresses in the steel fibers reach the ultimate bond strength, the tensile stresses in the steel fiber cannot be increased beyond this bond stress level. Most types of steel fibers actually reach their bond strengths before they reach their tensile strength as the crack widths increase. Therefore, in order to describe the failure mode of SFRC accurately, such pull-out failure of steel fibers at the crack interface should be considered in analytical model. Based on test results, Lim *et al*. (1987) proposed the maximum crack width of SFRC members, as follows:

$$w_{\max} = \frac{L_f}{16} \tag{28}$$

where L_f is the length of the steel fiber. The crack width of SFRC member (w_{sfrc}) can be estimated by

$$w_{sfrc} = s_{m\theta}\varepsilon_n^c q \tag{29}$$

where $s_{m\theta}$ is the average crack spacing, which is estimated by the method proposed by Collins and Mitchell (1991) in this study. q is the coefficient of crack control capacity, for which $50/\left(L_f/D\right)$ was used as proposed by Dupond and Vandewalle (2003). Thus, the proposed analysis in this study consider that the pull-out failure would occur when the estimated crack width (w_{sfrc}), defined in Eq. (29), exceeds the maximum crack width of SFRC ($w_{\max}$), presented in Eq. (28).

7. Validations of the proposed nonlinear finite element analysis

Fig. 9 shows the mesh details and the boundary condition of the finite element used in the analysis. To minimize mesh-dependency problem in the finite element analysis, as pointed out by Crisfield and Wills (1989) and Susetyo *et al*. (2013), only one element was used in finite element analysis. In addition, since no post-peak behavior was observed in the shear responses from panel tests as shown in Fig. 10, the analyses were performed by the load control method that can significantly reduce computational time without any loss of accuracy. In Fig. 10, the analysis results based on the proposed fixed-angle numerical analysis model are compared to the experimental test results of the SFRC panels tested under pure shear at the University of Toronto (Susetyo 2009, Susetyo *et al*. 2011 and 2012). The material properties, dimensional details, and observed and estimated shear capacities of panel specimens are summarized in Table 1. The key parameters of the test program included compressive strength of concrete, types of steel fibers, and the volume fraction of steel fibers, and a more detailed information on the test program can be found in elsewhere (Susetyo 2009, Susetyo *et al*. 2011 and 2013). The convergence condition of the nonlinear analysis in all loading stages was considered such that the ratio between the secant modulus in the previous stage (*i*-1) and that in the current stage (*i*), as shown in Eq. 19, would be less than 1%. Moreover, as previously explained, the failure criteria of SFRC members was determined such that the pullout failure would occur if the crack width (w_{sfrc}) in the fixed crack direction reached the maximum crack width ($w_{\max}$).

Shown in Figs. 10(a) to (e) are comparisons of the analysis results with the test results of C1-series specimens. The concrete compressive strengths of C1-series specimens were ranged from 45.5 to 51.4 MPa, and various types of steel fibers were used, in which the lengths of the steel fibers were 30 mm to 50 mm, their diameters were ranged from 0.38 mm to 0.62 mm. Furthermore, the fiber volume fractions of the specimens were between 0.5% and 1.5%. The analysis results showed that, after the stress in the steel fiber reached the maximum bond stress, the shear stiffness of the panels significantly decreases, and, finally, it was estimated by proposed model that the pull-out failures at the crack interface were occurred. The proposed model provided the shear behaviors

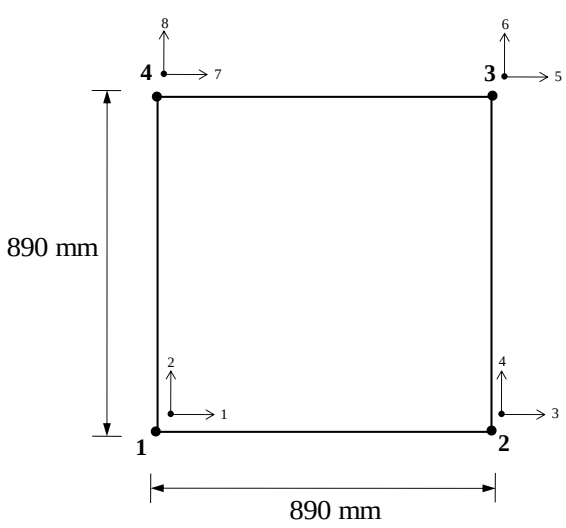

(a) Mesh and dimensions of panels

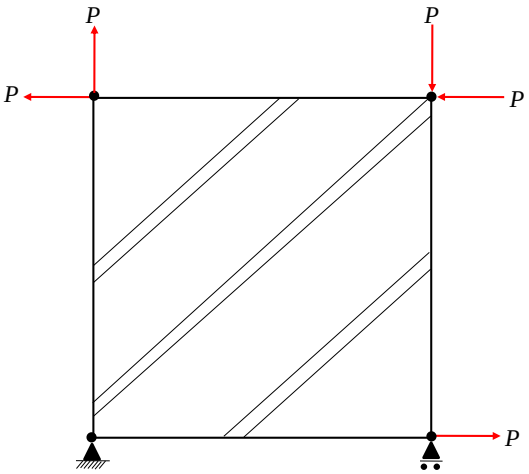

(b) Loading and boundary conditions

Fig. 9 Analysis details of panel specimens

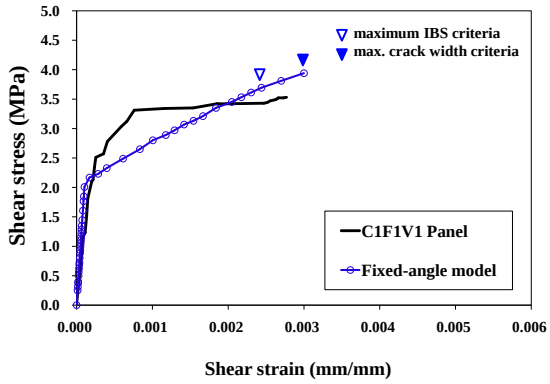

(a) C1F1V1 panel

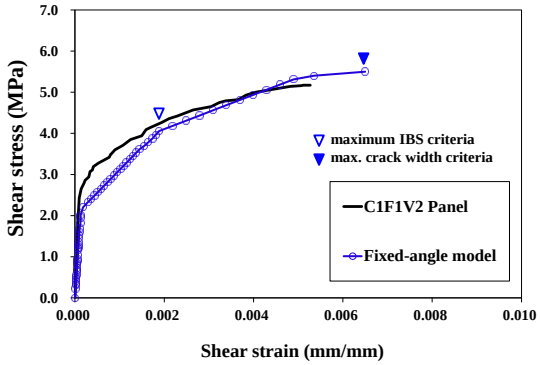

(b) (b) C1F1V2 panel

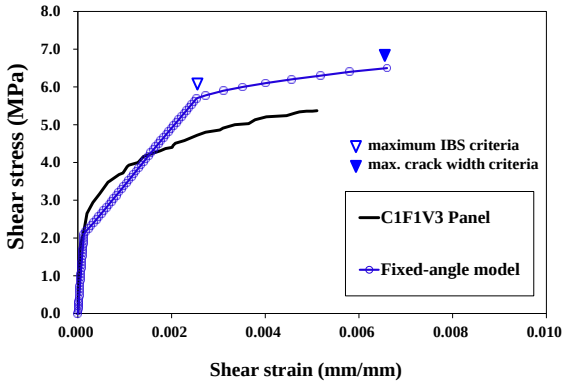

(c) C1F1V3 panel

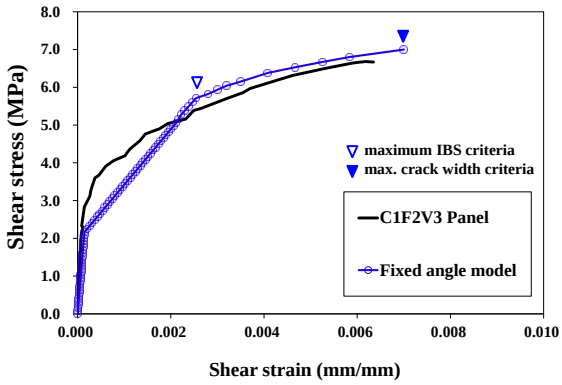

(d) C1F2V3 panel

Fig. 10 Validations of shear behavior of the proposed NLFEA with DTFTM

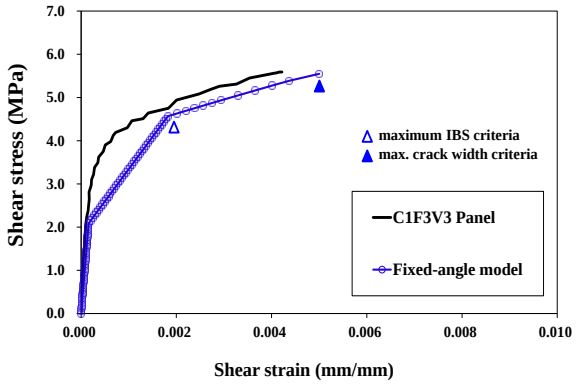

(e) C1F3V3 panel

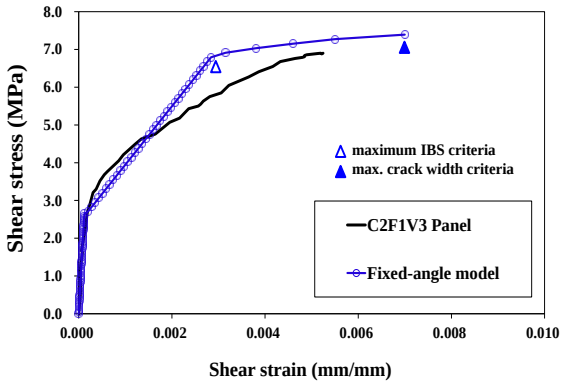

(f) C2F1V3 panel

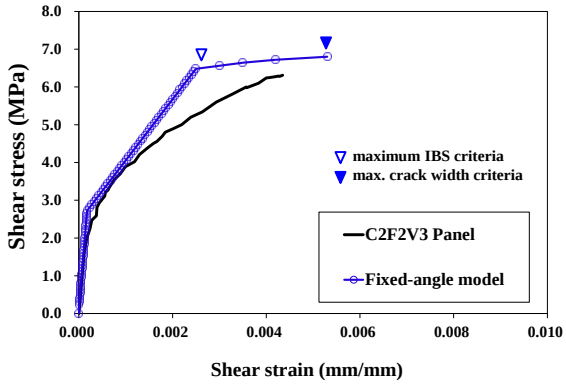

(g) C2F2V3 panel

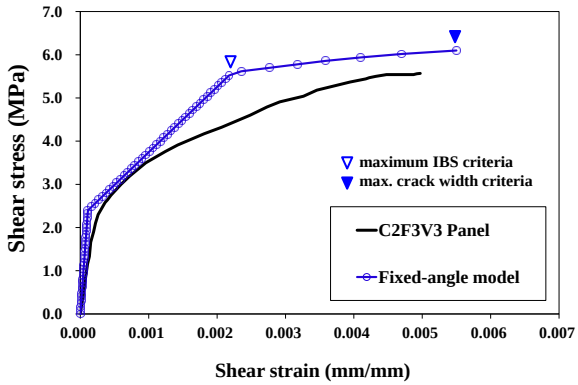

(h) C2F3V3 panel

Fig. 10 Continued

Table 1 Summary of panel specimens (Susetyo 2009)

Specimen names	Failure mode	Concrete		Steel fiber				Shear capacity		
		f_c' (MPa)	ε_{cu}' ($\times 10^{-3}$)	f_{fu} (MPa)	L (mm)	D (mm)	V_f (%)	v_{test} (MPa)	v_{cal} (MPa)	$\frac{v_{test}}{v_{cal}}$
C1F1V1	Interlock failure	51.4	2.150	1050	50	0.62	0.5	3.53	3.95	0.89
C1F1V2	Interlock failure	53.4	2.670	1050	50	0.62	1.0	5.17	5.50	0.94
C1F1V3	Interlock failure	49.7	2.500	1050	50	0.62	1.5	5.37	6.50	0.83
C1F2V3	Interlock failure	59.7	3.280	2300	30	0.38	1.5	6.68	6.95	0.96
C1F3V3	Interlock failure	45.5	2.340	1100	35	0.55	1.5	5.59	5.60	1.00
C2F1V3	Interlock failure	79.4	2.770	1050	50	0.62	1.5	6.90	7.35	0.94
C2F2V3	Interlock failure	76.5	2.220	2300	30	0.38	1.5	6.31	6.90	0.91
C2F3V3	Interlock failure	62.0	2.030	1100	35	0.55	1.5	5.57	6.00	0.93

Note: Size of panel, yield strength, and amount of longitudinal bar are 890 mm x 890mm x 70mm, 2063 mm^2(ρ_{sx} = 3.31%) and 552 MPa, in all specimens, respectively, v_{test} and v_{cal} are the observed and estimated shear capacity, respectively.

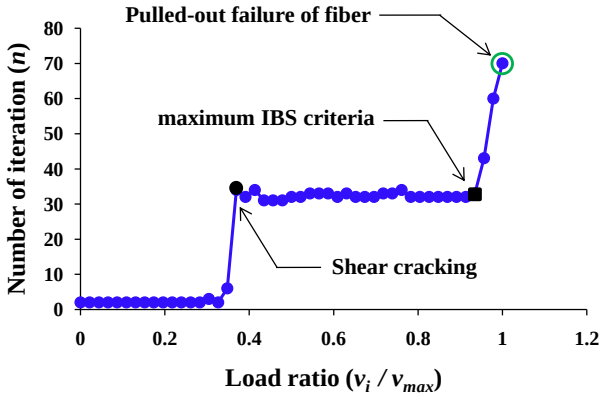

Fig. 11 Number of iteration to obtain the 1% convergence in the proposed model

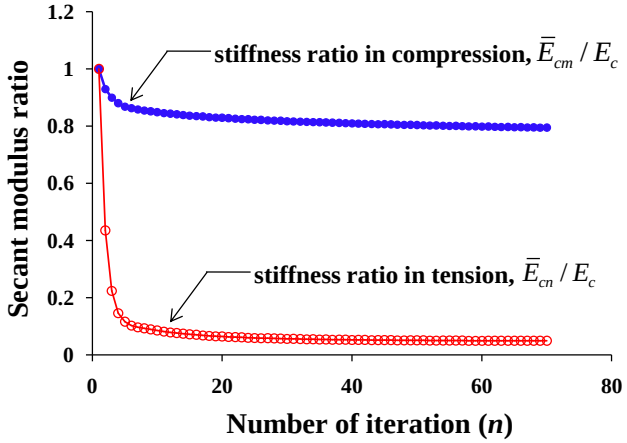

Fig. 12 Convergence characteristics of the proposed model at ultimate

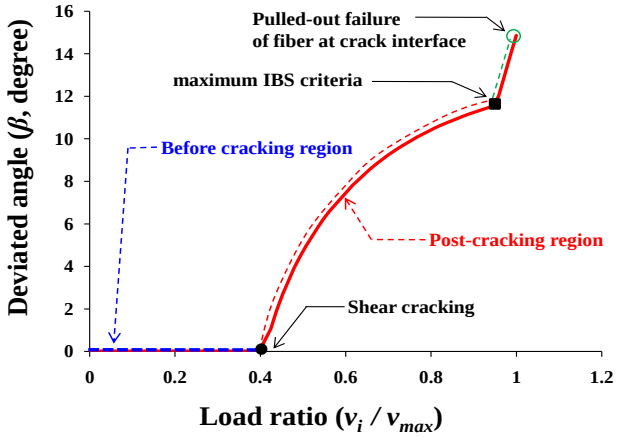

Fig. 13 Deviation angles in the proposed fixed-angle model with DTFTM

of SFRC members that were well agreed to the test results of C1-series specimens, and the point at which the failure occurred was also quite accurately predicted. While the proposed model effectively evaluated the shear stiffness of C1F1-series specimens with a large fiber aspect ratio (L/D) before the cracking [refer to Fig. 10(a) to (c)], it rather underestimated shear stiffness right after the shear cracking. Moreover, the proposed model overestimated the shear strengths of these specimens by 10 to 15% and their deformation capacities were slightly overestimated as well. Such a tendency was a little stronger when the volume fraction of fiber was larger. On the contrary, as shown in Figs. 10(d) and (e), the proposed model provided good estimations of the shear strengths and deformation capacities of the specimen CIF2V3 - the fiber aspect ratio used is almost similar to that of C1F1-series specimens, but the length and diameter of the fiber are smaller than those of C1F1 specimens - and the specimen C1F3V3 whose fiber aspect ratio was smaller by about 20%.

Figs. 10(f) to (h) show the comparisons of the analysis results with test results of C2-series specimens. C2-series specimens were cast with high-strength concrete, and their concrete compressive strengths were ranged from 62.0 MPa to 79.4 MPa. The fiber dimensions were 30 to 50 mm in length and 0.38 to 0.62 mm in diameter. The fiber volume fraction of all C2-series specimens was 1.5%. As with C1-series specimens, the proposed model also reasonably estimated the overall shear behavior of these C2-series specimens. In particular, the proposed model estimated the shear cracking strength very accurately, compared to the analysis results of the C1-series specimens. It tended to overestimate the shear stiffness after the shear cracking though, implying that the linear stress-strain relationship of steel fibers may need a modification such that the actual bond behavior of steel fibers before the maximum bond strength can be reflected in the analysis model, in addition to the consideration on the maximum bond strength of steel fibers. For these shear panel specimens cast with high-strength concrete, the analysis model rationally reflected the influences of fiber shapes (or fiber aspect ratios) on the shear behavior of SFRC member. However, it showed somewhat overestimations on the shear strength of the specimens, and as with the previous C1-series specimens, the proposed model also tended to slightly overestimate the deformation capacity of SFRC shear panels as the fiber aspect ratio is larger and the fiber length is longer.

Shown in Fig. 11 is the number of iterations performed at each loading stage in order to achieve 1% of convergence level in the analysis of C2F3V3 specimens, as an example of numerical stability. Before shear cracking, the numerical calculations were converged within 10 or less iterations because the SFRC members have elastic behavior, after which it rapidly increased up to 35 iterations due to the initiation of tensile contribution of the steel fiber at the crack interface. After the stresses in the steel fibers reached the maximum bond stress, the number of iteration again increased significantly, and at the point of pull-out failure of steel fibers, about 70 iterative computations were performed. The number of iterations required in this analysis is larger than that with rotating-angle theory, which had been reported in the previous studies (Lee *et al*. 2012, Vecchio 1989 and 1990). This implies that, if the fixed-angle theory is applied to the finite element analysis, a more careful numerical considerations are required than the rotating-angle model. Fig. 12 shows the convergence process of the secant moduli of C2F3V3 specimens at ultimate state, which confirms that the secant modulus method used in this study provides very stable convergence for the finite element analysis method adopting the fixed-angle model.

Fig. 13 shows the deviation angles between the principal stress direction and the fixed-crack direction of C2F3V3 specimens estimated by the proposed model at all loading stages. Before shear cracking, the principal stress direction was identical to the crack direction, and as soon as

cracking occurred, it increased rapidly in a nonlinear manner. After the stresses in steel fibers reached the maximum bond stress, the deviation angle increased more sharply, and it showed about 15 degrees at pull-out failure, which is due to the asymmetrical distribution of reinforcing bars in the specimen. Despite all the SFRC panel specimens used for validation in this study had reinforcing bars only in longitudinal direction, their deviation angles were very similar to the RC shear panels reinforced in both direction, which were estimated to have the deviation angles of 9 to 19 degrees of deviation angles in previous studies (Pang and Hsu 1996, Wang and Hsu 2001). It is believed that this is due to the tensile contribution of the steel fibers in the direction of the crack surface plane. It can be expected that the rotation-angle theory would estimate the pull-out failure of steel fibers to be occurred earlier than estimated by the fixed-angle theory because it does not consider the deviation angle. Thus, the consideration method on the crack direction would give a huge effect on determination of the deformation capacity of SFRC members (Susetyo *et al*. 2011). Moreover, while the assumption that the principal stress direction is identical to the crack direction make it difficult to consider the shear contribution of concrete, it should be noted that the shear contribution of concrete and steel fibers at the crack surface can be more reasonably considered in this analysis by utilizing the fixed-angle theory.

As explained above, based on the comparisons between analysis and test results of SFRC panels with various test variables, such as concrete compressive strength (f_c'), the volume fraction of steel fiber (V_f), and fiber aspect ratio (L/D), it was validated that the proposed numerical analysis model can estimate the shear strength and behavior of SFRC members accurately. Particularly, the pull-out failure criteria introduced in this study was suitable for estimation of the deformation capacity of SFRC members, and it was verified that this simple criterion can be applied to the analysis of high-strength SFRC members as well.

8. Conclusions

This study developed a nonlinear finite element analysis algorithm utilizing the fixed-angle theory and the direct tension transfer model to estimate the shear strength and behavior of SFRC members. As opposed to existing studies, this study considered steel fibers as a direct tension member in developing the evaluation model for the shear behavior of SFRC members. Based on the comparison between the results from the proposed model and the shear panel tests, the following conclusions can be drawn:

• The proposed fixed-angle model with DTFTM is a rational approach that can describe directionality, bond strength, and pull-out failure of fibers in a simple manner.

• The proposed model accurately estimated the cracking strength, ultimate shear strength, and failure mode of SFRC panels having various concrete compressive strength or different types of fibers.

• Deformation capacities of SFRC members were estimated quite accurately by the pull-out criteria of the proposed model with the consideration of deviation angle.

• The secant moduli method applied to the fixed-angle model provided very stable and fast convergence.

• The deviation angle, which caused the fundamental difference between the rotation-angle theory and the fixed-angle theory, significantly increased after shear cracking, and soared even more steeply after the stresses in the steel fibers reached maximum bond strength.

• The analysis results implied that the shear strength and behavior of SFRC members may be underestimated without consideration of the deviation angle.

Acknowledgements

This research was supported by a grant (12 High-tech Urban C04) from High-tech Urban Development Program funded by Ministry of Land, Transport and Maritime Affairs of Korean government.

References

Abrishami, H.H. and Mitchell, D. (1997), "Influence of steel fibers on tension stiffening", *ACI Struct. J.*, **94**(6), 769-776.

ACI-ASCE Committee 445 on Shear and Torsion (1999), "Recent approaches to shear design of structural concrete", *J. Struct. Engr.*, ASCE, **124**(12), 1375-1417.

ACI Committee 544 (1988), "Design consideration for steel fiber reinforced concrete (ACI 544.4R-88)", *ACI Struct. J.*, **85**(5), 563-580.

Bathe, K.J. (1996), *Finite Element Procedure*, Prentice-Hall, Upper Saddle River, NJ.

Chen, W.F. (1982), *Plasticity in Reinforced Concrete*, McGraw-Hill, USA.

Collins, M.P. and Mitchell, D. (1991), *Prestressed Concrete Structures*, Prentice Hill, Englewood Cliffs, NJ, USA.

Crisfield, M.A. and Wills, J. (1989), "Analysis of R/C panels using different concrete models", *J. Engr. Mech.*, ASCE, **115(**3), 578-597.

Dupont D. and Vandewalle, L. (2003), "Calculation of crack widths with the s-e method", *Test and Design Methods for Steel Fibre Reinforced Concrete: Background and Experiences - Proceedings of the RILEM TC162-TDF Workshop*, RILEM Technical Committee 162-TDF, Bochum, Germany, 119-144.

Hwang, J.H., Lee, D.H., Kim, K.S., Ju, H. and Seo, S.Y. (2012), "Evaluation of shear performance of steel fiber-reinforced concrete beams using a modified smeared-truss model", *Mag. Concrete Res*., **65**(5), 283-296.

Hwang, J.H., Lee, D.H., Ju, H.J., Kim, K.S. Seo, S.Y. and Kang, J.W. (2013), "Shear behavior models of steel fiber-reinforced concrete beams modifying softened truss model approaches", *Materials, Special Publication: Constitutive model on composite materials*, **6**(10), 4847-4867.

Hu, H. and Schnobrich, W.C. (1990), "Nonlinear analysis of cracked reinforced concrete", *ACI Struct. J.*, **87**(2), 199-207.

Hsu, T.T.C. (1998), "Stresses and crack angles in concrete membrane elements", *J. Struct. Eng., ASCE*, **124(**12), 1476-1484.

Hsu, T.T.C. and Mo, Y.L. (2010), Unified Theory of Concrete Structures, Wiley and Sons, USA.

Janis, O. (2008), "New frontiers for steel fiber-reinforced concrete", *Concrete Int.*, **30**(5), 45-50.

Ju, H., Lee, D.H., Hwang, J.H., Kang, J.W., Kim, K.S. and Oh, Y.H. (2013), "Torsional behavior model of steel fiber-reinforced concrete members modifying fixed-angle softened-truss model", *Comp. Part B: Eng.*, **45**(1), 215-231.

Ju, H., Lee, D.H., Hwang, J.H., Kim, K.S. and Oh, Y.H. (2013), "Fixed-angle smeared-truss approach with direct tension force transfer model for torsional behavior of steel fiber-reinforced concrete members", *J. Adv. Concrete Tech.*, **11**(1), 215-229.

Kim, J.Y., Park, H.G. and Yi, S.T. (2011), "Plasticity model for directional nonlocality by tension cracks in concrete planar members", *Engr. Struct.*, **33(**3), 1001-1012.

Kim, K.S., Lee, D.H., Hwang, J. and Kuchma, D.A. (2012), "Shear behavior model for steel fiber-reinforced concrete members without transverse reinforcements", *Comp. Part B: Eng*., **43**(5), 2324-2334.

Lee, D.H., Hwang, J.H., Ju, H., Kim, K.S. and Kuchma, D.A. (2012), "Nonlinear finite element analysis of steel fiber-reinforced concrete members using direct tension force transfer model", *Finite Elem. Anal. Des.*, **50**(1), 266-286.
Lee, J.Y., Kim, S.W. and Mansur, M.Y. (2011), "Nonlinear analysis of shear-critical reinforced concrete beams using fixed angle theory", *J. Struct. Engr*, ASCE, **137**(10), 1017-1029.
Lee, S.C., Cho, J.Y. and Vecchio, F.J. (2011), "Diverse embedment model for steel fiber-reinforced concrete in tension: model development", *ACI Mat. J.*, **108**(5), 516-525.
Lim, T.Y., Paramsivam, P. and Lee, S.L. (1987), "Analytical model for tensile behavior of steel-fiber concrete", *ACI Mat. J.*, **84**(4), 286-298.
Logan, D.L. (2007), *A First Course in the Finite Element Method*, 4th Ed., Thomson, Toronto, ON, Canada.
Narayanan, R. and Darwish, I.Y.S. (1987), "Use of steel fibers as shear reinforcement", *ACI Struct. J.*, **84**(3), 216-227.
Neville, A.M. (1996), *Properties of Concrete*, 4th ed., Wiley and Sons, London, UK.
Ngo, D. and Scordelis, A.C. (1967), "Finite element analysis of reinforced concrete beams", *ACI J. Proceedings*, **64**(3), 152-163.
Pang, X.D. and Hsu, T.T.C. (1996), "Fixed angle softened truss model for reinforced concrete", *ACI Struct. J.*, **93**(2), 197-207.
Popovics, S. (1973), "A numerical approach to the complete stress-strain curve and concrete", *Cement Concrete Res.*, **3**(5), 583-599.
Romualdi, J.P. and Mandel, J.A. (1964), "Tensile strength of concrete affected by uniformly distributed and closely spaced short lengths of wire reinforcement", *ACI J., Proceeding*, **61**(6), 657-671.
Smith, I.M. and Griffiths, D.V. (2004), *Programming the Finite Element Analysis*, (4th Ed. John Wiley and Sons), Hoboken, NJ, USA.
Soroushian, P. and Lee, C.D. (1990), "Distribution and orientation of fibers in steel fiber reinforced concrete", *ACI Mat. J.*, **87**(5), 433-439.
Susetyo, J. (2009), "Fibre reinforcement for shrikage crack control in prestressed, precast segmental bridges", Ph.D dissertation, University of Toronto, Toronto, ON, Canada.
Susetyo, J., Gauvreau, P. and Vecchio, F.J. (2011), "Effectiveness of steel fiber as minimum shear reinforcement", *ACI Struct. J.*, **108**(4), 488-496.
Susetyo, J., Gauvreau, P. and Vecchio, F.J. (2013), "Steel fiber-reinforced concrete panels in shear: analysis and modeling", *ACI Struct. J.*, **110**(2), 285-295.
Tan, K.H. and Mansur, M.A. (1990), "Shear transfer in steel fiber concrete", *J. Mat. Civ. Eng.*, ASCE, **2**(4) 202-214.
Tan, K.H., Murugappan, K. and Paramasivam, P. (1992), "Shear behavior of steel fiber reinforced concrete beams", *ACI Struct. J.*, **89**(6), 3-11.
Vecchio, F.J. (1989), "Nonlinear finite element analysis of reinforced concrete membranes", *ACI Struct. J.*, **86**(1), 26-35.
Vecchio, F.J. (1990), "Reinforced concrete membrane element formulation", *J. Struct. Eng., ASCE*, **116**(3), 730-750.
Vecchio, F.J. and Collins, M.P. (1986), "Modified compression field theory for reinforced concrete elements subjected to shear", *ACI J. Proceedings*, **83**(2), 219-231.
Voo, J.Y.L. and Foster, S.J. (2003), *Variable Engagement Model for Fibre Reinforced Concrete in Tension*, UNICIV Report No. R-420 June 2003, University of New South Wales, Sydney, Australia, 1-86.
Wang, T. and Hsu, T.T.C. (2001), "Nonlinear finite element analysis of concrete structures using new constitutive models", *Comput. Struct.*, **79**(32), 2781-2791.
Yang, T.Y. (1986), *Finite Element Structural Analysis*, Prentice-Hall, Englewood Cliffs, NJ, USA.

CC